Lb-miR166a has a potentially positive impact on the treatment of kidney cancer

Qiang Zhang
Ningxia Medical College: Ningxia Medical University
Zhiyuan Xie
Ningxia Medical College: Ningxia Medical University https://orcid.org/0000-0002-2952-5826
Yan Li
Ningxia Medical College: Ningxia Medical University
Qian Zhu
Ningxia Medical College: Ningxia Medical University
Hongbin Shi
Ningxia Medical College: Ningxia Medical University
Ruining Zhao
Ningxia Medical College: Ningxia Medical University
Xiaobo Yang
Ningxia Medical College: Ningxia Medical University
Jia Tian (tianjia113@126.com)
https://orcid.org/0000-0001-7366-6661
Lianghong Ma
Ningxia Medical College: Ningxia Medical University

Research article

Keywords: Renal cell carcinoma, Lycium barbarum, Lycium barbarum miRNA166a, Targeted drugs

Posted Date: June 21st, 2022

DOI: https://doi.org/10.21203/rs.3.rs-1740960/v1

Abstract

Background

Renal cell carcinoma (RCC) is the seventh most common tumor worldwide. The incidence rate of RCC ranks second among urinary system tumors, and the incidence rate has been increasing in recent years. Recent studies have shown that plant miRNAs can be absorbed into organisms through diet, and can regulate target gene expression and physiological function of predators across species. As a traditional Chinese medicine, *Lycium barbarum* has a wide range of antitumor effects. However, there are no reports on the cross-border regulation of tumors by *Lycium barbarum* miRNA (*Lb*-miRNA).

Methods

Human RCC cells (Caki-1) were cultured in vitro. The overexpression group of *Lb*-miR166a was constructed using lentivirus transfection. The effect of *Lb*-miR166a on the expression of RCC cells was analyzed using transcriptome sequencing, and differentially expressed genes were screened. Combined with bioinformatics technology, the relevant mechanisms by which *Lb*-miR166a regulates the occurrence and development of RCC were screened and verified, and *in vivo* tumor-bearing experiments on nude mice verified the effect of *Lb*-miR166a expression on the occurrence, development, invasion, and metastasis of RCC.

Results

Transcriptome sequencing analysis showed that *Lb*-miR166a regulated the expression of a variety of genes in tumor cells and regulated a large number of signaling pathways related to tumor occurrence and development. The overall finding was that *Lb*-miR166a inhibited tumor cell proliferation, promoted tumor cell apoptosis, and inhibited cell invasion and metastasis. The tumor-bearing experiment in nude mice also showed that the subcutaneous tumor formation volume decreased in *Lb*-miR166a group mice, as did the expression of tumor cell Ki67 and the number of liver metastases.

Conclusion

This study explains the role of *Lb*-miR166a in the treatment of RCC and its underlying mechanisms. These results further improve the antitumor mechanism of *L. barbarum* and provide ideas for the clinical development of targeted drugs for the treatment of RCC.

Background

Renal cell carcinoma (RCC) is the seventh most common tumor worldwide. Its incidence rate in men is higher than that in women. RCC ranks second among urological tumors in terms of incidence rate. In

recent years, the incidence has increased. In 2018, approximately 400,000 people worldwide were diagnosed with RCC [1]. RCC tissue types include clear cell carcinoma (70%), papillary cell carcinoma (10–15%), and chromophobe cell carcinoma (5%). The treatment methods for RCC include surgery, chemoradiotherapy, and endocrine therapy, but the curative effect remains poor [2]. Surgical resection can be cured. Unfortunately, 25–30% of patients have distant metastasis at the time of diagnosis, and approximately 40% of patients relapse after surgical resection [3]. In recent years, great progress has been made in research on the occurrence, development, treatment, and prognosis of renal cancer. There are traces of related drugs, animal, and plant compounds, nanomaterials, and non-coding RNA in the treatment of renal cancer, laying a foundation for the targeted treatment of renal cancer.

In recent years, some studies have found a type of non-self miRNA in animals. This miRNA mainly enters food and plays a regulatory role in animals. miRNAs are endogenous, coding single stranded RNA widely present in organisms. Because of their special structure or coating of exosomes, plant miRNAs are absorbed by animals into the body of predators, which still have certain stability and tissue specificity, and can regulate the target gene expression and physiological function of predators across species [4, 5]. This type of RNA does not encode any proteins. It affects the expression of target genes by combining with the 3'-UTR terminal sequence of target genes [6] and then regulates biological processes, including cell growth, tissue development, cell proliferation, differentiation, apoptosis, invasion, and metastasis [7]. It plays an important regulatory role in a variety of diseases, particularly tumors. However, the biological roles of most exogenous plant miRNAs remain unclear.

Ningxia *Lycium barbarum* is a traditional Chinese herbal plant that is widely used as a functional food and medicinal material to promote health and longevity in China and other Asian countries. Currently, it is a food with the characteristics of a natural dietary supplement and low-affinity drug [8]. The main components of *Lycium barbarum* include polysaccharides, flavonoids, carotenoids, and betaine [9]. They have the functions of regulating oxidative stress and inflammation, reducing blood lipid, delaying aging, and promoting antioxidation and antitumor activities [10, 11]. However, there are no reports on the cross-border regulation of tumors by *Lycium barbarum* miRNA (*Lb*-miRNA).

Therefore, we designed this study to further study the role and mechanism of *Lb*-miR166a in the treatment of renal cell carcinoma.

Materials And Methods

Cell culture

Caki-1 cells were purchased from Procell Life Science & Technology Co., Ltd. (Wuhan, China), and cultured in McCoy's 5A medium (Procell Life Science & Technology Co., Ltd.) containing 10% fetal bovine serum (Biological Industries, Beit-Haemek, Israel) and 1% penicillin–streptomycin liquid (Beijing Solarbio Science & Technology Co., Ltd., Beijing, China) at 37 °C in a humidified environment consisting of 5% CO_2.

Lentivirus transfection and cell grouping

Caki-1 cells at the logarithmic growth stage were subcultured in 6-well plates, with 10^5 cells in each well. After 24 h, cells were divided into a normal control group (N-Con), and transfected with the control lentivirus for the lentivirus control group (L-Con). The *Lb*-miR166a mimic group cells were transfected with *Lb*-miR166a mimic lentivirus.

mRNA sequence analysis

mRNA sequence analysis of total RNA extracted from N-Con and *Lb*-miR166a cells was performed at Wuhan GeneCreate Biological Engineering Co., Ltd. (Wuhan, China). Samples were prepared using a TruSeq Stranded mRNA Library Prep Kit (Illumina, San Diego, CA, USA), according to the manufacturer's protocol. The library was prepared by adding adapters to the fragmented RNA samples. The library was 303–314 bp in length. Sequencing of the clusters formed in the S4 flow cell was performed using the NovaSeq 6000 (Illumina), a next-generation sequencer. The effective read length was 100 bp, and analysis was performed using the paired-end/multiplex method.

Cell cycle analysis

Cell cycle analysis was performed using propidium iodide (PI). In brief, the cells were gently trypsinized and washed twice with cold phosphate-buffered saline (PBS), at least 1×10^6 cells were fixed in 70% ethanol overnight at 4 °C. After the removal of the ethanol, the cells were incubated with 400 μL PI at 4 °C for 30 min, and the cell cycle was assessed using flow cytometry.

Apoptosis assay

Transfected Caki-1 cells were seeded in 6-well plates (1×10^6 cells/well). Following transfection, cells were harvested using centrifugation at 200 × *g* for 5 min, washed with 1× PBS three times, and then incubated with 5 μL of FITC-conjugated Annexin V and 5 μL PI (25 μg/mL) (both BD Biosciences, San Jose, CA, USA) for 15 min at room temperature in the dark. Stained cells were detected using a BD FACSAria II flow cytometer (BD Biosciences). FlowJo V10.5.2 (BD Biosciences) was used to analyze the data.

Western blot

RIPA buffer was used to extract the total protein from the cultured cells. Following extraction, bicinchoninic acid assays (Beyotime Biotechnology, Shanghai, China) were performed to quantify all proteins. Equal amount of protein samples was separated by 8%–12% sodium dodecyl sulfate–polyacrylamide gel electrophoresis and then transferred to the nitrocellulose membranes (Millipore, Burlington, MA, USA). The membranes were blocked with 5% nonfat milk/PBS for 1 h and then incubated with primary antibodies at 4 °C overnight. After washing the membranes with PBS containing 1% Tween 20 three times, they were incubated with secondary antibodies for 2 h. The membranes were developed using an enhanced chemiluminescence solution (Beyotime Biotechnology) and exposed to a

photographic film for visualization. An additional table lists the antibodies used in this study (Supplementary Table 1).

Quantitative real-time PCR (qRT–PCR) assay

Total RNA was extracted from tissues and cell lines using TRIzol reagent (TianGen, Beijing, China), and RNA quality was assessed using NanoDrop 2000c (Thermo Fisher Scientific, Waltham, MA, USA). Next, the RNA was converted into cDNA using a RevertAid First Strand cDNA Synthesis Kit (Thermo Fisher Scientific), and qRT–PCR was conducted on an ABI 7900 system using SYBR Green Real-Time PCR Master Mixes (Thermo Fisher Scientific) under the following reaction conditions: 95 °C for 3 min, followed by 40 cycles of 95 °C for 30 s, 60 °C for 30 s, and 75 °C for 30 s. GAPDH served as an internal control. The primers were synthesized by RiboBio (Guangzhou, China). The transcriptional levels of target genes were analyzed using the $2^{-\Delta\Delta Ct}$ method. The sequences of all primers were listed in Supplementary Table 2.

Wound healing assay

Briefly, cells (1×10^5) were seeded in six-well plates and incubated overnight. A wound was created with a 10 μL pipette tip, and images were obtained under a light microscope (Zeiss Corpi, Shanghai, China). The wound gaps were measured at each time point.

Transwell assay

Transwell chambers (six-well; 8 μm; Corning Inc., Corning, NY, USA) were used for migration and invasion analyses, and partial chambers were coated with Matrigel (BD Biosciences). A total of 4×10^4 cells placed in serum-free culture medium were added to the top of the chambers with or without Matrigel for invasion or migration analysis, respectively. The bottom of the chambers was filled with a culture medium containing 10% fetal bovine serum to induce cell migration or invasion. After 24 h, the cells on the lower surface were fixed with 4% paraformaldehyde and stained with 0.1% crystal violet (Beyotime Biotechnology). Five randomly selected areas were used for observation and the cells were counted under an inverted microscope (100×; Olympus, Tokyo, Japan).

Metastasis Assay In Vivo

Nude mouse xenografted with Caki cells/*in vivo* assays

A total of 24 healthy nude mice 4–6 weeks old were raised in a specific-pathogen-free animal laboratory with humidity of 60%–65% at 22–25 °C. The animals were provided free access to food and water under a 12 h light/dark cycle.

Twelve nude mice were subcutaneously injected with N-Con or *Lb*-miR166a cells (1×10^8) (n = 6/group). After 6 weeks, the nude mice were euthanized and the tumor volume was recorded.

Twelve nude mice were used to establish an *in vivo* metastasis model. Caki-1 cells (1×10^7) stably overexpressing *Lb*-miR166a or N-Con were injected into the tail vein of mice (n = 6/group). After 8 weeks, the mice were sacrificed, and their livers were photographed. The tumor nodules on the surface of the liver were counted separately by two researchers.

Immunohistochemistry

The subcutaneous tumors of mice in each group were fixed with 4% paraformaldehyde, dehydrated with gradient ethanol, paraffin embedded after transparent treatment with xylene, sliced into 5 μm slices, dewaxed with xylene, rehydrated, and antigen repaired. Next, 0.3% Triton-100 was used to permeate the cell membrane for 15 min, after which it was washed with PBS thrice, incubated with 3% H_2O_2 at room temperature for 15 min, and washed with PBS thrice again. Ki67 protein expression in the tumor tissue was detected using the streptavidin peroxidase method, followed by 3,3'-diaminobenzidine (DAB) chromogenic solution, hematoxylin restaining the nucleus, blue reversion, dehydration, and neutral adhesive sealing. The SP-9001 Immunohistochemical Staining Kit and the ZLI-9018 DAB kit were purchased from ZSGB-BIO (Beijing, China).

Statistical analysis

All data were analyzed with SPSS 21.0 and presented as mean ± SD. Two-tailed paired and unpaired Student's *t*-tests were used to test for significant differences between two groups. One-way analysis of variance followed by Tukey's test was used for multi-sample analysis. $P < 0.05$ was considered significant. GraphPad Prism software (version 7.0) was used for the drawing.

Result

Detection of *Lb*-miR166a expression in RCC cells

qRT-PCR showed that *Lb*-miR166a was not expressed in RCC cells and L-Con group cells, whereas the expression of *Lb*-miR166a was significantly upregulated in *Lb*-miR166a group cells. This shows that the transferred *Lb*-miR166a could be successfully expressed in tumor cells (Figure 2).

Transcriptome sequencing and differential gene screening analysis

The Hisat2 software was used to compare the reads obtained from the sequencing data with the reference genome for similarity analysis. By quickly comparing each "read" with the reference genome sequence, the position and matching quality of the "read" on the compared genome or other reference sequences are finally obtained, and the gene or transcript can be annotated and quantified. A total of 19,225 gene entries were measured in this study.

There were differences in the gene expression among the different samples. Based on the comparison results, the differential expression of genes in each sample was analyzed using edgeR software, and the adjusted *P* (*P*adj) value of differential expression was calculated. The *P*adj value indicated that the gene

expression difference was more significant. In this experiment, genes with |log2 fold change| ≥ 1 and *P*adj < 0.05 were selected as significant differentially expressed genes. The differences in mRNA expression between the two groups were statistically analyzed. A total of 1,813 differentially expressed mRNAs were screened. Cluster analysis of differentially expressed mRNAs showed that 1,232 mRNAs were significantly upregulated and 581 were significantly downregulated (Figure 3a).

To better understand the biological function of differentially expressed mRNA, we analyzed the differentially expressed mRNA using GO. A total of 1,813 differentially expressed genes were annotated into 1,094 GO entries, of which 1,074 were significantly enriched ($P < 0.05$), including 605 physiological process entries, 44 cell component entries, and 48 molecular function entries (Figure 3b).

The differentially expressed genes were enriched in 43 KEGG pathways, of which 30 were significantly enriched ($P < 0.05$). It can be seen that the upregulated genes were enriched in tumor-related cell adhesion molecules and apoptosis; the downregulated genes were significantly enriched in cell proliferation and other pathways (Figure 3c).

Lb-miR166a regulates hsa05200 pathway gene expression

Hsa05200 (a pathway in cancer) has been identified as the most important pathway in tumor pathogenesis. The activation of many genes and signaling pathways plays a key role in tumor cell proliferation and differentiation; apoptosis; and tumor infiltration, growth, recurrence, and metastasis.

Through differential gene annotation, as shown in Figure 4, *Lb*-miR166a can regulate the expression of multiple genes of hsa05200 pathway in cancer, so as to regulate tumorigenesis and development.

Lb-miR166a inhibits proliferation of Caki-1 cells

Cell proliferation depends mainly on the normal operation of the cell cycle. Mitosis entering the cell cycle is strictly controlled by the promotion or inhibition of growth signals, which are important for cell proliferation and division. To further clarify the effect of *Lb*-miR166a on cell proliferation-related genes and pathways, we screened out cell proliferation-related differential genes based on gene function annotation and constructed a circular heat map. There were 88 proliferation-related differential genes in the *Lb*-miR166a group compared with the N-Con group, including 29 upregulated genes and 59 downregulated genes (Figure 5a).

The above differentially expressed proliferation genes were annotated and analyzed by GO and KEGG enrichment analysis, and 6 proliferation-related GO entries and 1 KEGG pathway were enriched ($P < 0.05$), as shown in Figure 5b,c.

To verify the effect of *Lb*-miR166a on cell proliferation, we first evaluated the proliferation activity of the three groups using a Cell Counting Kit-8 cell proliferation assay. The results showed that the cell optical density value in the *Lb*-miR166a group was significantly lower than that in the N-Con and L-Con groups ($P < 0.05$), whereas there was no significant difference between the N-Con and L-Con groups ($P > 0.05$;

Figure 6a). The results showed that *Lb*-miR166a significantly inhibited renal cell viability. Simultaneously, we compared the cell cycle distribution of the three groups using flow cytometry (Figure 6b,c). The results showed that the proportion of cells in the G0/G1 phase increased in the *Lb*-miR166a group, whereas the proportion of cells in the S and G2/M phases decreased, indicating that the cells in the *Lb*-miR166a group were blocked in the G0/G1 phase. Western blotting showed that the expression levels of ID4, CCND2, CCNB1, CCNA2, CDC20, and CCNE2 in the *Lb*-miR166a group were downregulated ($P < 0.05$); this trend was consistent with the results of transcriptome sequencing (Figure 6d,e).

Lb-miR166a promotes apoptosis of Caki-1 cells

Apoptosis is a process of spontaneous programmed cell death, which is closely related to the occurrence and development of tumors. To further clarify the effect of *Lb*-miR166a on apoptosis-related genes and pathways, we screened out apoptosis-related differential genes based on gene function annotation and drew a circular heat map. It can be seen that there were 89 differential genes in the *Lb*-miR166a group compared with the N-Con group, including 60 upregulated and 29 downregulated apoptosis-related genes (Figure 7a).

The above differentially expressed apoptosis genes were annotated and analyzed by GO and KEGG pathways, and 11 apoptosis-related GO entries and one KEGG pathway were enriched ($P < 0.05$), as shown in Figure 7b,c.

To verify the effect of *Lb*-miR166a on RCC cell apoptosis, we compared the apoptosis rates of the three groups using flow cytometry. The results showed that the apoptosis rate of the *Lb*-miR166a group was significantly higher than that of the N-Con and L-Con groups ($P < 0.05$); however, there was no significant difference between the N-Con and L-Con groups ($P > 0.05$) (Figure 8a,b).

We then detected the protein expression of apoptosis-related genes in the three groups of cells using western blotting. The results showed that the *Lb*-miR166a group inhibited the downregulation of the expression of the apoptosis protein Bcl2 ($P < 0.05$), while the expression levels of the apoptosis proteins Bad and Bax and the content of the cleaved Caspase-3 protein in the cells were significantly upregulated ($P < 0.05$); this trend was consistent with the transcriptome sequencing results (Figure 8c,d).

Gene interaction network reveals the effect of *Lb*-miR166a on cell apoptosis and proliferation

By selecting the key GO and KEGG pathways for cell proliferation and apoptosis, we demonstrated the effect of *Lb*-miR166a on the gene table of proliferation and apoptosis of RCC cells through the gene protein–protein interaction network. The squares in the figure represent different GO and KEGG pathways and the dots represent genes. Red indicates that the expression of the *Lb*-miR166a group is upregulated compared with that of the N-Con group, and green indicates that the expression of the *Lb*-miR166a group is downregulated compared with that of the N-Con group (Figure 9).

Lb-miR166a inhibits cell metastasis and invasion

Migration/invasion, the key initial step in tumor cell metastasis, is of great significance in the occurrence and development of tumors. To further verify the effect of *Lb*-miR166a on the migration and invasion of RCC cells, we determined the scratch healing rate of the three groups using a cell scratch experiment. The results showed that the scratch healing rate of cells in the *Lb*-miR166a group decreased significantly compared to that of those in the N-Con and L-Con groups ($P < 0.05$; Figure 10a,b).

The Transwell invasion experiment showed that compared to those in the N-Con and L-Con groups, the number of cancer cells migrating to the lower compartment in the *Lb*-miR166a group decreased significantly ($P < 0.05$). These results showed that *Lb*-miR166a inhibited the migration and invasion of RCC cells (Figure 10c,d).

Lb-miR166a inhibits tumor proliferation and metastasis in nude mice

The tumor-bearing experiment in nude mice showed that the subcutaneous tumor forming volume in the *Lb*-miR166a group was significantly smaller than that in the N-Con group ($P < 0.05$) (Figure 11a,b). The number of liver metastases in the *Lb*-miR166a group was significantly lower than that in the N-Con group ($P < 0.05$) (Figure 11c,d). Immunohistochemical detection of subcutaneous tumorigenesis in nude mice showed that the expression of Ki67 was decreased in the subcutaneous tumorigenesis of the *Lb*-miR166a group mice (Figure 11e,f).

Discussion

Phytochemicals contain a variety of substances, including plant polyphenols, saponins, polysaccharides, and other bioactive substances. Edible plants contain not only nutrients and phytochemicals but also plant miRNAs. For a long time, scientists believed that plant miRNAs cannot avoid the degradation of the animal digestive tract; that is, plant miRNAs cannot exist stably in animals, so they ignored the possibility of animals obtaining and using dietary plant miRNA. Recent research [12], however, showed that the degradation rate of animal miRNA was much higher than that of the plant miRNA control group when animal miRNA and plant miRNA were placed in a solution simulating the acidic environment in the stomach (pH 2.0). The above study showed that the unique post-synthesis methylation modification of plant miRNAs could help them to maintain their stability and avoid their rapid degradation in acidic environments. Through this mechanism, plant miRNAs can successfully avoid erosion in the acidic environment of the digestive tract and enter the circulatory system through the animal gastrointestinal tract. A large number of recent studies have also shown that miRNAs can be transmitted between different species, especially between plants and animals [13], and plant-derived miRNAs can stably exist in animal blood [14], breast milk [15, 16], and tissues and organs [17], and play a role in regulating the expression of a variety of target proteins [14, 18]. An increasing number of studies have also found that plant miRNAs can prevent or even treat human diseases, including cardiovascular diseases [19], tumors [20, 21], chronic inflammation [22], and pulmonary fibrosis [23].

In this study, we introduced *Lb*-miR166a into RCC cells. Through sequencing, we found that 1,813 gene mRNAs were differentially expressed in the *Lb*-miR166a group compared to those in the N-Con group. Cluster analysis was carried out on the differentially expressed mRNA, of which 1,232 were significantly upregulated and 581 were significantly downregulated. Through differential gene annotation analysis, it was found that *Lb*-miR166a can regulate cell proliferation, apoptosis, and adhesion, as well as the gene expression levels in the NF-κB signaling pathway, the TGF-β signaling pathway, and multiple other pathway.

Inhibiting the proliferation rate of RCC cells is the most important goal in the treatment of RCC [24]. Tumor cells, particularly malignant tumor cells, proliferate faster, and cell proliferation and apoptosis are affected by the cell cycle. Therefore, regulating the tumor cell cycle, inhibiting the proliferation of tumor cells, and promoting their apoptosis are the main targets for tumor treatment [25]. The cell cycle in eukaryotic cells is mainly regulated by two essential factors: cyclins (CCN) and cyclin-dependent kinases (CDKs) [26].

In this study, *Lb*-miR166a downregulated the expression of CCNA2, CCND1, CCNE2, CCNB1, and cell division cycle 20 (CDC20). At the same time, cell cycle analysis showed that the proliferation ability of Caki-1 cells decreased after the transfection of *Lb*-miR166a. Cell cycle analysis showed that the proportion of G0/G1 phase cells increased, while the proportion of S and G2/M phase cells decreased, indicating that cells were blocked in the G0/G1 phase.

The G1/S phase is a key regulatory point in the cell cycle. When cells enter the S phase from G1, CCND/CDK4/6, CCNE/CDK2, and CCNA/CDK2 all play important roles. CCND1 enables cells to enter the S phase from G1 [27],which is also called the restriction point, and is the key to determining whether the cell cycle continues. The reduction in CCND1 plays a negative regulatory role in the G1/S cell cycle and blocks the cell cycle [28]. Studies have shown that CCNE2 is significantly increased in tumor-derived cells, including cervical cancer [29] and bladder cancer [30], and that the expression level of CCNE2 is negatively correlated with tumor grade and is significantly correlated with tumor growth pattern, invasiveness, and poor overall survival rate [31]. Decreasing CCNE2 expression in tumor cells may lead to G1/S cell cycle arrest [32]. Previous studies [33] have shown that CCNA2 is highly expressed in a variety of tumors, and it plays a key role in cell cycle control in the G1/S and G2/M phases by activating CDK4/6.

CCNB1 plays a key role in regulating the progression of the G2/M phase of the cell cycle. CCNB1 binds to CDK1 and forms the heterodimer CCNB1/CDK1, that is, the maturation promoting factor, which promotes cells from the G2 phase to the M phase and initiates mitosis. A large number of studies have also shown that CCNB1 expression in transplanted tumor cells can reduce cell proliferation, block the cell cycle in the G2/M phase, increase apoptosis, and inhibit tumorigenesis [34]. As a cell cycle checkpoint regulator, cell division cycle 20 (CDC20) is a regulatory protein that promotes complex/cyclic interactions in the late cell cycle and is involved in mitotic initiation [35]. Abnormal CDC20 levels or dysfunction can eliminate mitotic arrest, promote precocious activation proteins, and lead to aneuploidy changes in progeny cells. Many

studies have shown that the increased expression of CDC20 is related to adverse pathological features and prognosis of many human cancers [36, 37].

Apoptosis is a non-inflammatory and active death process formed by multicellular organisms to maintain homeostasis. It also involves the expression and regulation of multiple genes [38]. There are two core signaling pathways in apoptosis: the exogenous death receptor signaling pathway, which is activated by extracellular death signals, and the endogenous mitochondrial signaling pathway, which is activated by intracellular stress [39].

Bcl-2 and Bax, members of the Bcl-2 protein family, are important cytokines that regulate apoptosis. Bcl-2 mainly inhibits apoptosis, whereas Bax promotes apoptosis [40]. When stimulated by the cell death signal, Bax can upregulate the release of apoptotic factors and induce apoptosis, whereas Bcl-2 inhibits apoptosis in this process [41]. Caspase-3 is a member of the caspase family and is a key molecule that regulates apoptosis [42]. Activation of caspase-3 can promote apoptosis, and its degree of activation is an important indicator for evaluating apoptosis [43]. This study showed that compared with N-Con tissues, *Lb*-miR166a screened 89 apoptosis-related differential genes, including 60 upregulated and 29 downregulated genes. Differential gene annotation analysis showed that 11 apoptosis-related GO entries and 1 KEGG pathway were enriched. Apoptosis-related analysis showed that the apoptosis rate of cells in the *Lb*-miR166a group increased and the expression of the *Bcl2* gene was downregulated, while the expression of apoptotic proteins Bad and Bax and the cleaved caspase-3 protein content in cells were significantly upregulated, indicating that *Lb*-miR166a can promote the apoptosis of RCC cells.

Lb -miR166a inhibits invasion and metastasis of RCC cells

Tumor metastasis refers to the formation of secondary tumors by tumor cells migrating from the primary site to other parts of the body through lymphatic and blood vessels. This process includes separation from the primary focus, survival in the circulatory system, and distant regrowth [44]. In this study, we used a scratch test to detect the effects of *Lb*-miR166a on cell metastasis. The results showed that compared to the N-Con group, the cell metastasis ability of the *Lb*-miR166a group was significantly limited ($P < 0.05$), indicating that mir-166a can inhibit the migration of RCC cells. The Transwell cell invasion assay was used to detect the effect of *Lb*-miR166a on cell invasion. The results showed that compared to the N-Con group, the cell invasion ability of the *Lb*-miR166a group was significantly limited ($P < 0.05$), indicating that mir-166 can inhibit the invasion of RCC cells.

Tumor-bearing experiments in nude mice verified the effect of *Lb*-miR166a on the biological behavior of RCC cells *in vivo*, and showed that the tumor volume in the *Lb*-miR166a group was significantly reduced. Immunohistochemical analysis showed that the Ki67 protein expression in the *Lb*-miR166a group was downregulated, and the number of liver metastases in the *Lb*-miR166a group was significantly lower than that in the N-Con group.

Conclusions

This study preliminarily showed, using transcriptome sequencing, that *Lb*-miR166a promotes renal cancer cell apoptosis and inhibits cell proliferation, invasion, and metastasis through the cross-border regulation of gene expression in renal cancer cells. The results of this study suggest that *Lb*-miR166a could be important for the treatment of renal cancer; however, its specific molecular mechanism, drug development, and biological prediction still require extensive research and exploration and clinical trials will be needed to verify the safety and effectiveness of the drug.

Abbreviations

RCC
Renal cell carcinoma
Lb-miRNA
Lycium barbarum miRNA
Caki-1
Human RCC cells
PBS
phosphate-buffered saline
GO
Gene Ontology
KEGG
Kyoto Encyclopedia of Genes and Genomes
CDC20
cell division cycle 20
CDKs
cyclin-dependent kinases
CCN
Cyclin

Declarations

Ethics declarations

All animal experiments were performed in accordance with the guidelines of the Ethical Committee of the General Hospital of Ningxia Medical University.

Consent for publication

Not applicable.

Availability of data and materials

All data generated or analyzed in this study are included in this published article and its supplementary information files. Please contact the authors of this article for more information.

Competing interests

The authors declare that they have no competing interests.

Funding

Not applicable.

Authors' contributions

*These authors contributed equally to this study. #These authors contributed equally to this article and are corresponding authors.

QZ and JT designed the study, and reviewed the manuscript. QZ, ZYX, YL, and TJ performed the experiments and drafted the manuscript. ZYX, Qian Z and XBY performed the animal experiments and analyzed the data. HBS, RNZ, and LHM conceived the study, participated in its design and coordination, and helped to draft the manuscript. All of the authors have read and approved the final manuscript.

Acknowledgements

Not applicable.

Author's information

Affiliations

QZ, HBS, RNZ, XBY, LHM

Department of Urology, General Hospital of Ningxia Medical University, , No.804 Shengli South Street, Xingqing District, Yinchuan 750001, Ningxia Hui Autonomous Region, China.

ZYX, YL

Clinical College of Ningxia Medical University, No.804 Shengli South Street, Xingqing District, Yinchuan 750001, Ningxia Hui Autonomous Region, China.

Qian Z

Department of Medical Laboratory, Cardiovascular and Cerebrovascular Disease Hospital, General Hospital of Ningxia Medical University No.804 Shengli South Street, Xingqing District, Yinchuan 750001, Ningxia Hui Autonomous Region, China.

JT

Department of Human Sperm Bank of Ningxia, General Hospital of Ningxia Medical University, No.804 Shengli South Street, Xingqing District, Yinchuan 750001, Ningxia Hui Autonomous Region, China.

Author information

QZ (18810347@qq.com),

ZYX (xzy273500@163.com)

YL (liyandaxue@163.com)

Qian Z(527504941@qq.com)

HBS (Shb0525@163.com)

RNZ (zhaoruining5257@163.com)

XBY (yxb_0810@163.com)

JT (tianjia113@126.com)

LHM (mmm1770@163.com)

References

1. McCroskey Z, Sim SJ, Selzman AA, Ayala AG, Ro JY. Primary collision tumors of the kidney composed of oncocytoma and papillary renal cell carcinoma: a review. Ann Diagn Pathol. 2017;29:32-6.
2. Bray F, Ferlay J, Soerjomataram I, Siegel RL, Torre LA, Jemal A. Global cancer statistics 2018: GLOBOCAN estimates of incidence and mortality worldwide for 36 cancers in 185 countries. CA Cancer J Clin. 2018;68:394-424.
3. Kim SH, Park B, Hwang EC, Hong SH, Jeong CW, Kwak C, Byun SS, Chung J. Retrospective multicenter long-term follow-up analysis of prognostic risk factors for recurrence-free, metastasis-free, cancer-specific, and overall survival after curative nephrectomy in non-metastatic renal cell carcinoma. Front Oncol. 2019;9:859.
4. Stephen BJ, Pareek N, Saeed M, Kausar MA, Rahman S, Datta M. Xeno-miRNA in maternal-infant immune crosstalk: an aid to disease alleviation. Front Immunol. 2020;11:404.
5. Marzano F, Caratozzolo MF, Consiglio A, Licciulli F, Liuni S, Sbisà E, D'Elia D, Tullo A, Catalano D. Plant miRNAs reduce cancer cell proliferation by targeting MALAT1 and NEAT1: a beneficial cross-kingdom interaction. Front Genet. 2020;11:552490.
6. Cardoso AP, Udoh KT, States JC. Arsenic-induced changes in miRNA expression in cancer and other diseases. Toxicol Appl Pharmacol. 2020;409:115306.

7. Miao J, Regenstein JM, Xu D, Zhou D, Li H, Zhang H, Li C, Qiu J, Chen X. The roles of microRNA in human cervical cancer. Arch Biochem Biophys. 2020;690:108480.
8. Yao R, Heinrich M, Zou Y, Reich E, Zhang X, Chen Y, Weckerle CS. Quality variation of Goji (Fruits of *Lycium* spp.) in China: a comparative morphological and metabolomic analysis. Front Pharmacol. 2018;9:151.
9. Jin M, Huang Q, Zhao K, Shang P. Biological activities and potential health benefit effects of polysaccharides isolated from *Lycium barbarum* L.. Int J Biol Macromol. 2013;54:16-23.
10. Gao Y, Wei Y, Wang Y, Gao F, Chen Z. *Lycium barbarum*: a traditional Chinese herb and a promising anti-aging agent. Aging Dis. 2017;8:778-91.
11. Xiao Z, Deng Q, Zhou W, Zhang Y. Immune activities of polysaccharides isolated from *Lycium barbarum* L. What do we know so far?. Pharmacol Ther. 2022;229:107921.
12. Zhang L, Hou D, Chen X, Li D, Zhu L, Zhang Y, Li J, Bian Z, Liang X, Cai X, Yin Y. Exogenous plant MIR168a specifically targets mammalian LDLRAP1: evidence of cross-kingdom regulation by microRNA. Cell Res. 2012;22:107-26.
13. Ma J, Wang C, Long K, Zhang H, Zhang J, Jin L, Tang Q, Jiang A, Wang X, Tian S, Chen L. Exosomal microRNAs in giant panda (*Ailuropoda melanoleuca*) breast milk: potential maternal regulators for the development of newborn cubs. Sci Rep. 2017;7:3507.
14. Liang H, Zhang S, Fu Z, Wang Y, Wang N, Liu Y, Zhao C, Wu J, Hu Y, Zhang J, Chen X. Effective detection and quantification of dietetically absorbed plant microRNAs in human plasma. J Nutr Biochem. 2015;26:505-12.
15. Lukasik A, Zielenkiewicz P. In silico identification of plant miRNAs in mammalian breast milk exosomes—a small step forward?. PLoS One. 2014;9:e99963.
16. Lukasik A, Brzozowska I, Zielenkiewicz U, Zielenkiewicz P. Detection of plant miRNAs abundance in human breast milk. Int J Mol Sci. 2017;19.
17. Jia L, Zhang D, Xiang Z, He N. Nonfunctional ingestion of plant miRNAs in silkworm revealed by digital droplet PCR and transcriptome analysis. Sci Rep. 2015;5:12290.
18. Luo Y, Wang P, Wang X, Wang Y, Mu Z, Li Q, Fu Y, Xiao J, Li G, Ma Y, Gu Y. Detection of dietetically absorbed maize-derived microRNAs in pigs. Sci Rep. 2017;7:645.
19. Hou D, He F, Ma L, Cao M, Zhou Z, Wei Z, Xue Y, Sang X, Chong H, Tian C, Zheng S. The potential atheroprotective role of plant MIR156a as a repressor of monocyte recruitment on inflamed human endothelial cells. J Nutr Biochem. 2018;57:197-205.
20. Mlotshwa S, Pruss GJ, MacArthur JL, Endres MW, Davis C, Hofseth LJ, Peña MM, Vance V. A novel chemopreventive strategy based on therapeutic microRNAs produced in plants. Cell Res. 2015;25:521-24.
21. Chin AR, Fong MY, Somlo G, Wu J, Swiderski P, Wu X, Wang SE. Cross-kingdom inhibition of breast cancer growth by plant miR159. Cell Res. 2016;26:217-28.

22. Cavalieri D, Rizzetto L, Tocci N, Rivero D, Asquini E, Si-Ammour A, Bonechi E, Ballerini C, Viola R. Plant microRNAs as novel immunomodulatory agents. Sci Rep. 2016;6:25761.
23. Du J, Liang Z, Xu J, Zhao Y, Li X, Zhang Y, Zhao D, Chen R, Liu Y, Joshi T, Chang J. Plant-derived phosphocholine facilitates cellular uptake of anti-pulmonary fibrotic HJT-sRNA-m7. Sci China Life Sci. 2019;62:309-20.
24. Li Y, Quan J, Chen F, Pan X, Zhuang C, Xiong T, Zhuang C, Li J, Huang X, Ye J, Zhang F. MiR-31-5p acts as a tumor suppressor in renal cell carcinoma by targeting cyclin-dependent kinase 1 (CDK1). Biomed Pharmacother. 2019;111:517-26.
25. Ramos-García P, Bravo M, González-Ruiz L, González-Moles MÁ. Significance of cytoplasmic cyclin D1 expression in oral oncogenesis. Oral Dis., 2018;24:98-102.
26. Malumbres M, Barbacid M. Cell cycle, CDKs and cancer: a changing paradigm. Nature Rev Cancer. 2009;9:153-66.
27. Li Y, Peng L, Seto E. Histone deacetylase 10 regulates the cell cycle G2/M phase transition via a novel Let-7-HMGA2-Cyclin A2 pathway. Mol Cell Biol. 2015;35:3547-65.
28. Zhou C, Du J, Zhao L, Liu W, Zhao T, Liang H, Fang P, Zhang K, Zeng H. GLI1 reduces drug sensitivity by regulating cell cycle through PI3K/AKT/GSK3/CDK pathway in acute myeloid leukemia. Cell Death Dis. 2021;12:231.
29. Xiao L, Hong L, Zheng W. Motor neuron and pancreas homeobox 1 (MNX1) is involved in promoting squamous cervical cancer proliferation via regulating cyclin E. Med Sci Monitor: Int Med J Exp Clin Res. 2019;25:6304-12.
30. Wu Y, Zheng Q, Li Y, Wang G, Gao S, Zhang X, Yan X, Zhang X, Xie J, Wang Y, Sun X, Meng X, Yin B, Wang B. Metformin targets a YAP1-TEAD4 complex via AMPKα to regulate CCNE1/2 in bladder cancer cells. J Exp Clin Cancer Res, 2019;38:376.
31. Kanska J, Zakhour M, Taylor-Harding B, Karlan BY, Wiedemeyer WR. Cyclin E as a potential therapeutic target in high grade serous ovarian cancer. Gynecol Oncol. 2016;143:152-8.
32. Sheldon LA. Inhibition of E2F1 activity and cell cycle progression by arsenic via retinoblastoma protein. Cell Cycle, 2017;16:2058-72.
33. Gao T, Han Y, Yu L, Ao S, Li Z, Ji J. CCNA2 is a prognostic biomarker for ER+ breast cancer and tamoxifen resistance. PLoS One, 2014, 9(3): e91771.
34. Zhang H, Zhang X, Li X, Meng W-B, Bai Z-T, Rui S-Z, Wang Z-F, Zhou W-C, JinX-D. Effect of CCNB1 silencing on cell cycle, senescence, and apoptosis through the p53 signaling pathway in pancreatic cancer. J Cell Physiol. 2018;234:619-31.
35. Piano V, Alex A, Stege P, Maffini S, Stoppiello GA, Huis In 't Veld PJ, Vetter IR, Musacchio A. CDC20 assists its catalytic incorporation in the mitotic checkpoint complex. Science, 2021;371:67-71.
36. Wang L, Yang C, Chu M, Wang ZW, Xue B. Cdc20 induces the radioresistance of bladder cancer cells by targeting FoxO1 degradation. Cancer Lett. 2021;500:172-81.

37. Sun C, Li M, Feng Y, Sun F, Zhang L, Xu Y, Lu S, Zhu J, Huang J, Wang J, Hu Y, Zhang Y. MDM2-P53 signaling pathway-mediated upregulation of CDC20 promotes progression of human diffuse large B-cell lymphoma. Onco Targets Ther. 2020;13:10475-87.
38. Sauler M, Bazan IS, Lee PJ. Cell death in the lung: the apoptosis-necroptosis axis. Ann Rev Physiol. 2019;81:375-402.
39. Liu G, Pei F, Yang F, Li L, Amin A, Liu S, Buchan J, Cho W. Role of autophagy and apoptosis in non-small-cell lung cancer. Int J Mol Sci. 2017;18(2).
40. Flores-Romero H, Hohorst L, John M, Albert MC, King LE, Beckmann L, Szabo T, Hertlein V, Luo X, Villunger A, Frenzel LP, Kashkar H, Garcia-Saez AJ. BCL-2-family protein tBID can act as a BAX-like effector of apoptosis. EMBO J. 2022;41(2):e108690.
41. Aida R, Hagiwara K, Okano K, Nakata K, Obata Y, Yamashita T, Yoshida K, Hagiwara H. miR-34a-5p might have an important role for inducing apoptosis by down-regulation of SNAI1 in apigenin-treated lung cancer cells. Mol Biol Rep. 2021;48:2291-7.
42. An W, Lai H, Zhang Y, Liu M, Lin X, Cao S. Apoptotic pathway as the therapeutic target for anticancer traditional Chinese medicines. Front Pharmacol. 2019;10:758.
43. Means JC, Lopez AA, Koulen P. Resveratrol protects optic nerve head astrocytes from oxidative stress-induced cell death by preventing caspase-3 activation, tau dephosphorylation at Ser(422) and formation of misfolded protein aggregates. Cell Mol Neurobiol. 2020;40:911-26.
44. Atiya H, Frisbie L, Pressimone C, Coffman L. Mesenchymal stem cells in the tumor microenvironment. Adv Exp Med Biol. 2020;1234:31-42.

Figures

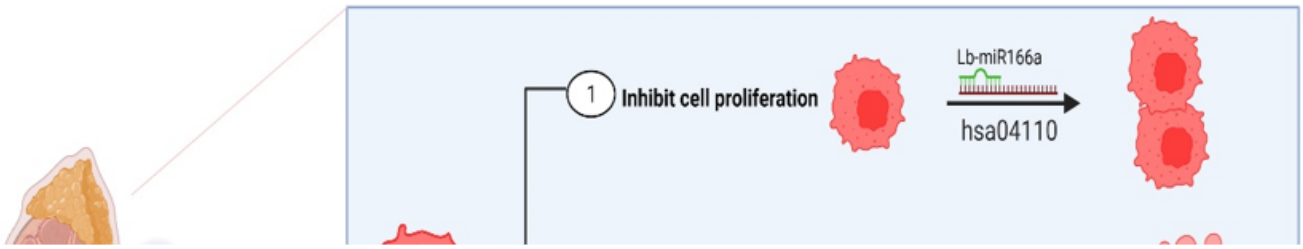

Figure 1

Lb-miR166a has a potentially positive impact on the treatment of kidney cancer

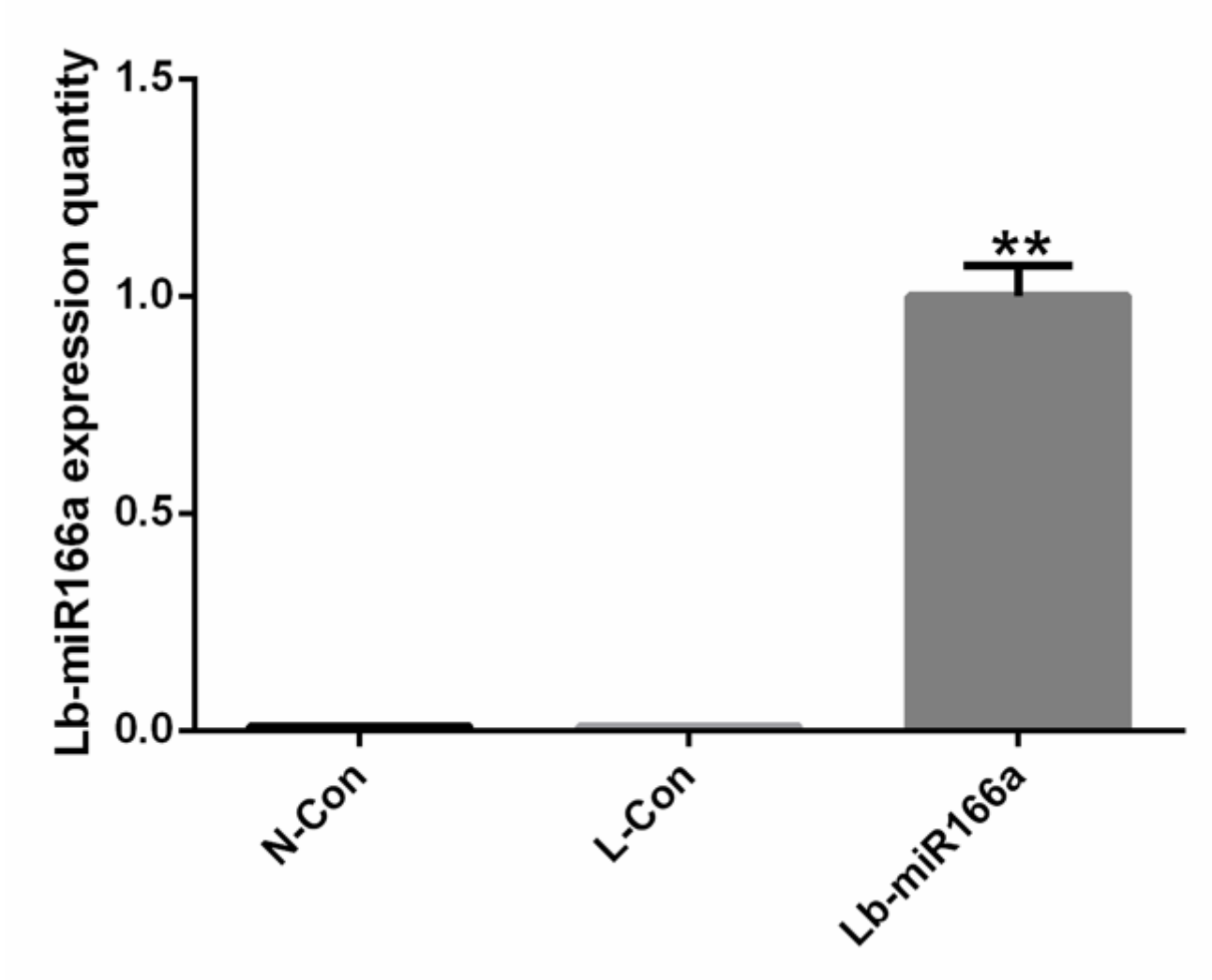

Figure 2

The expression of *Lb*-miR166a was detected by qRT-PCR（**P＜0.01）

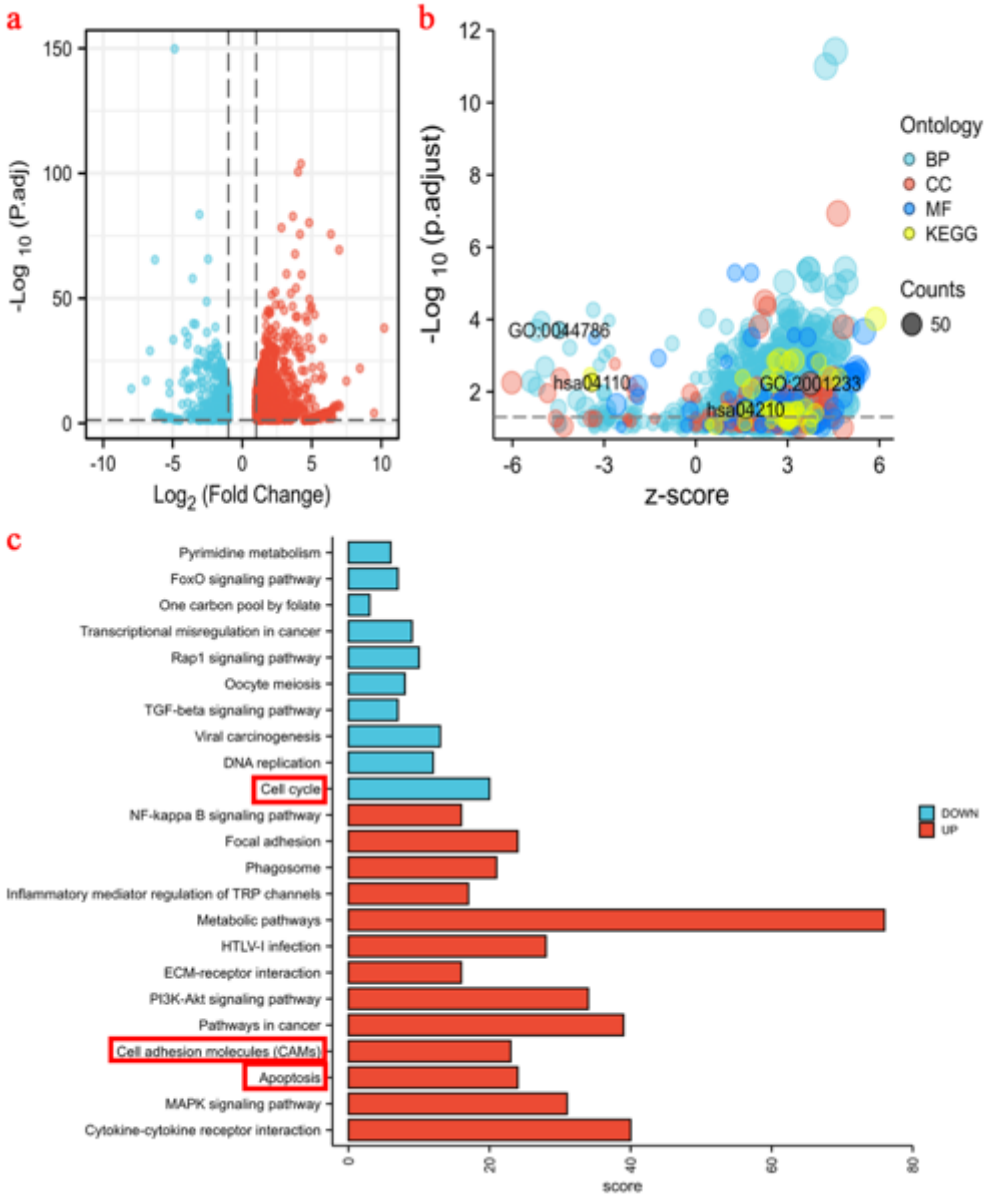

Figure 3

Screening and functional annotation of differential genes by transcriptome sequencing. a,Screening of differentially expressed genes, the total number of IDs after removing null values was 1813, among which, there were 1813 gene IDs meeting the threshold of log2 (FC) > 1 & p.adj < 0.05, 1232 gene IDs with high expression and 581 gene IDs with low expression. Red indicates significantly up-regulated genes and blue indicates significantly down-regulated genes. b, functional annotation of differentially expressed genes. c, enrichment analysis of tumor-related KEGG pathway, red indicates significantly up-regulated pathway, blue indicates significantly down-regulated pathway.

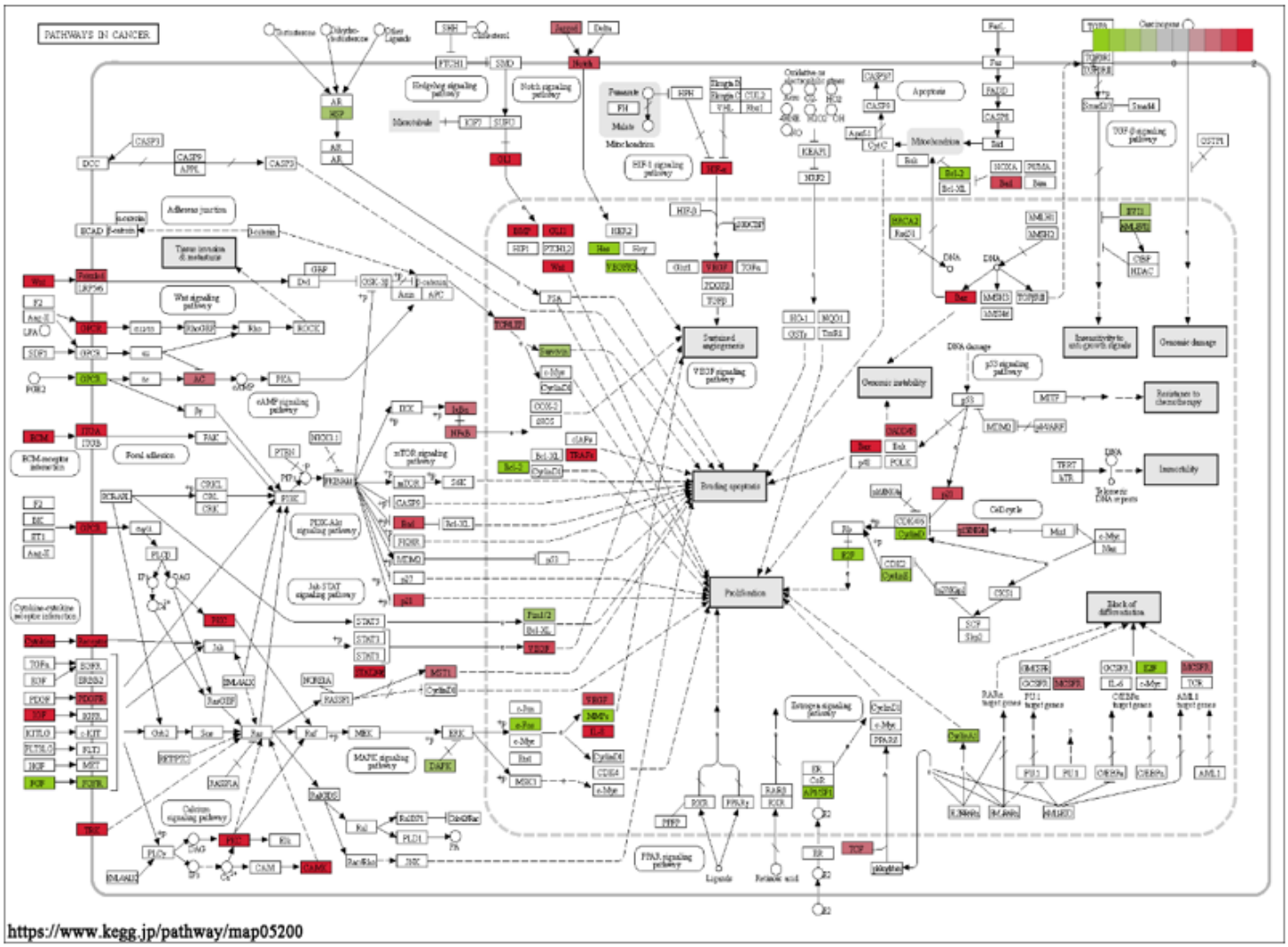

Figure 4

Hsa05200 (pathway in cancer) pathway differentially expressed gene annotation, red indicates significantly up-regulated gene, green indicates significantly down-regulated gene.

Figure 5

Lb -miR166a inhibits cell proliferation. a,Cell proliferation related gene expression notes: red indicates significant up regulation and blue indicates significant down regulation. b,Cell proliferation related go entries and KEGG pathway enrichment analysis, red indicates that the gene expression is significantly up-regulated in this pathway, and blue indicates that the gene expression is significantly down regulated in this pathway. C, Hsa04110 (cell cycle) pathway differentially expressed genes note: red indicates significantly up-regulated genes and green indicates significantly down-regulated genes

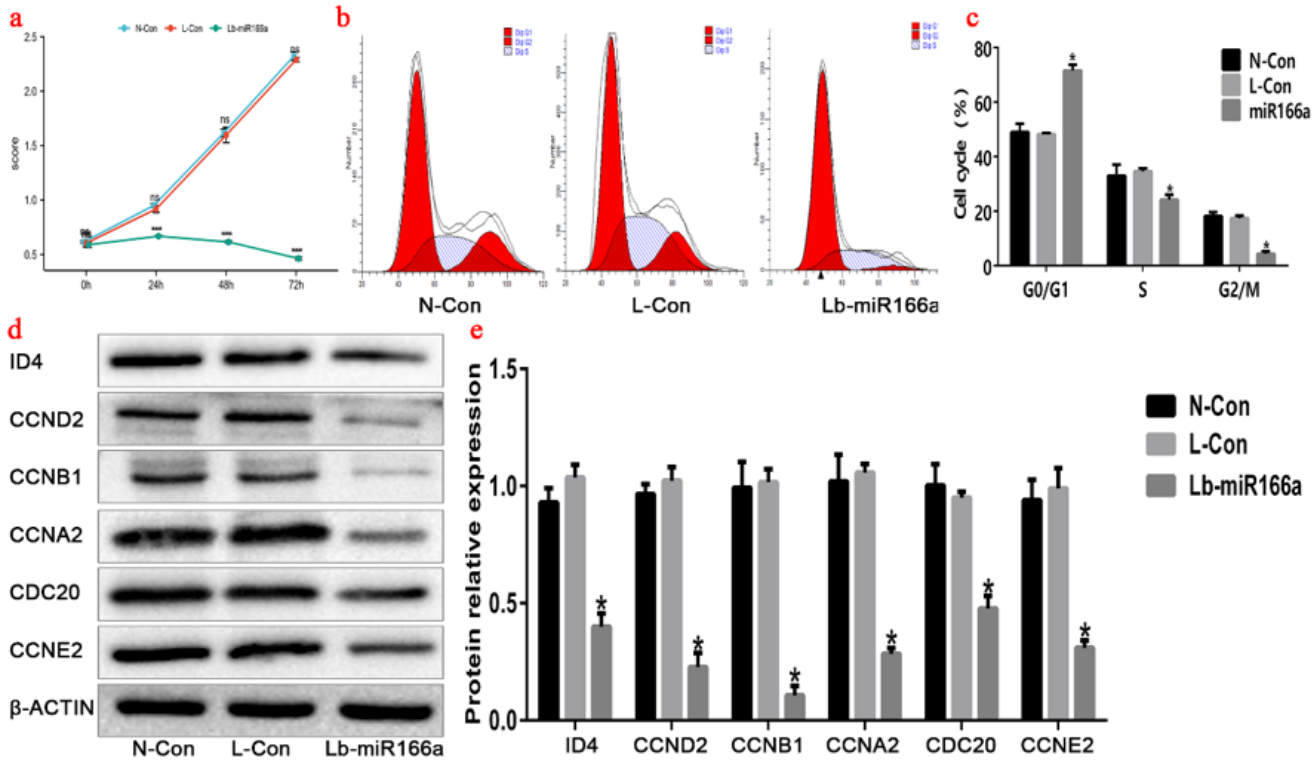

Figure 6

Lb-miR166a inhibited cell proliferation. a,b,c, Flow cytometry was used to detect cell cycle. d,e, Western blot was used to detect the expression of cell cycle-related genes and proteins. (*P<0.05).

Figure 7

Enrichment analysis of apoptosis-related pathways. a, Annotation of apoptosis-related gene expression, Red indicates significant up-regulation and blue indicates significant down-regulation. b, apoptosis-related GO items and KEGG pathway enrichment analysis, red indicates significant up-regulation of gene expression in this pathway, blue indicates significant down-regulation of gene expression in this pathway. c, hsa04210 (Apoptosis) pathway differentially expressed gene annotation, red indicates significant up-regulation of gene, green indicates significant down-regulation of gene.

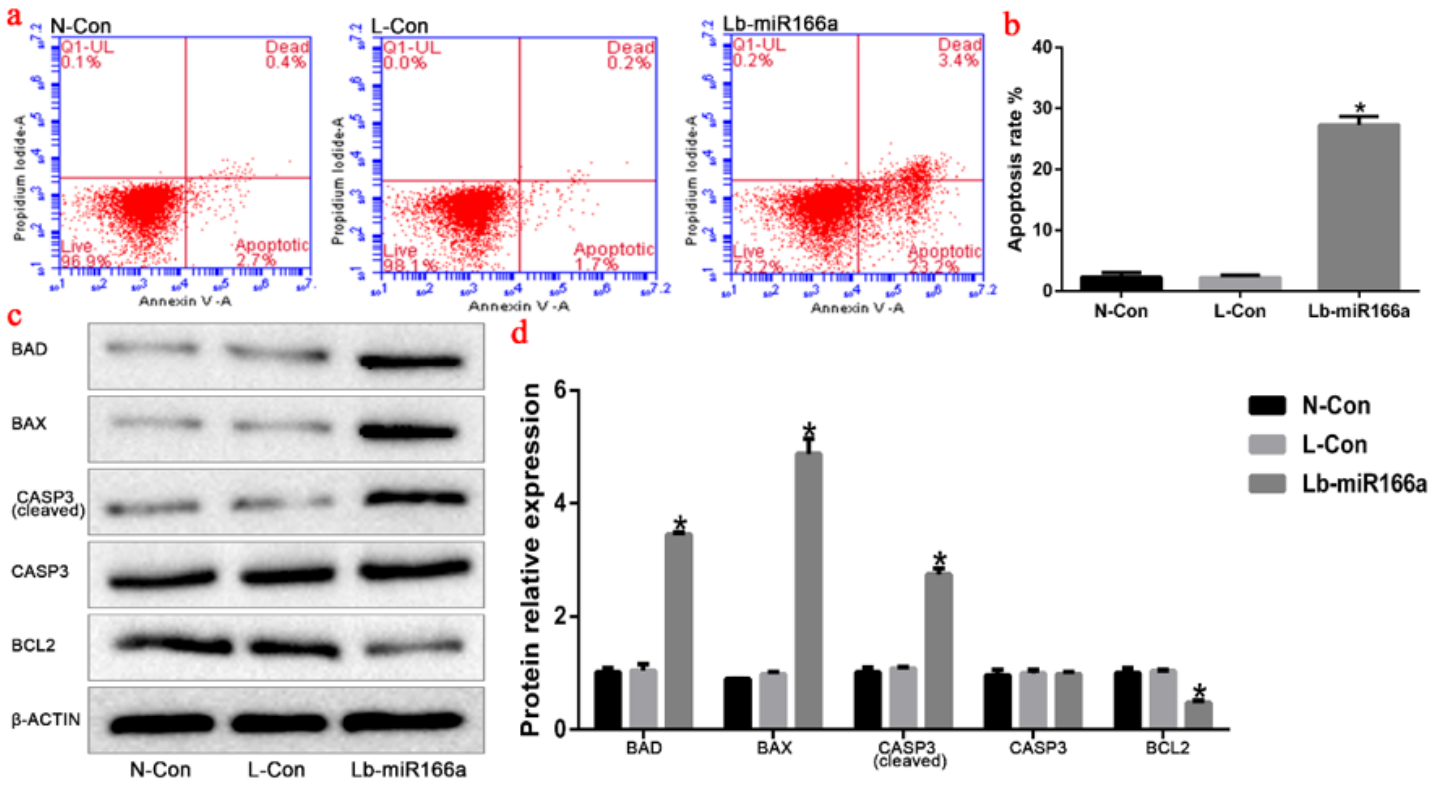

Figure 8

Lb-miR166a promoted the detection of apoptosis of renal cell carcinoma cells. a,b, Apoptosis was detected by flow cytometry. c,d, The expression of apoptosis related genes and proteins was detected by Western blot. (*P<0.05).

Figure 9

PPI network demonstrated the effect of *Lb*-miR166a on the gene expression of proliferation and apoptosis in renal cell carcinoma cells.

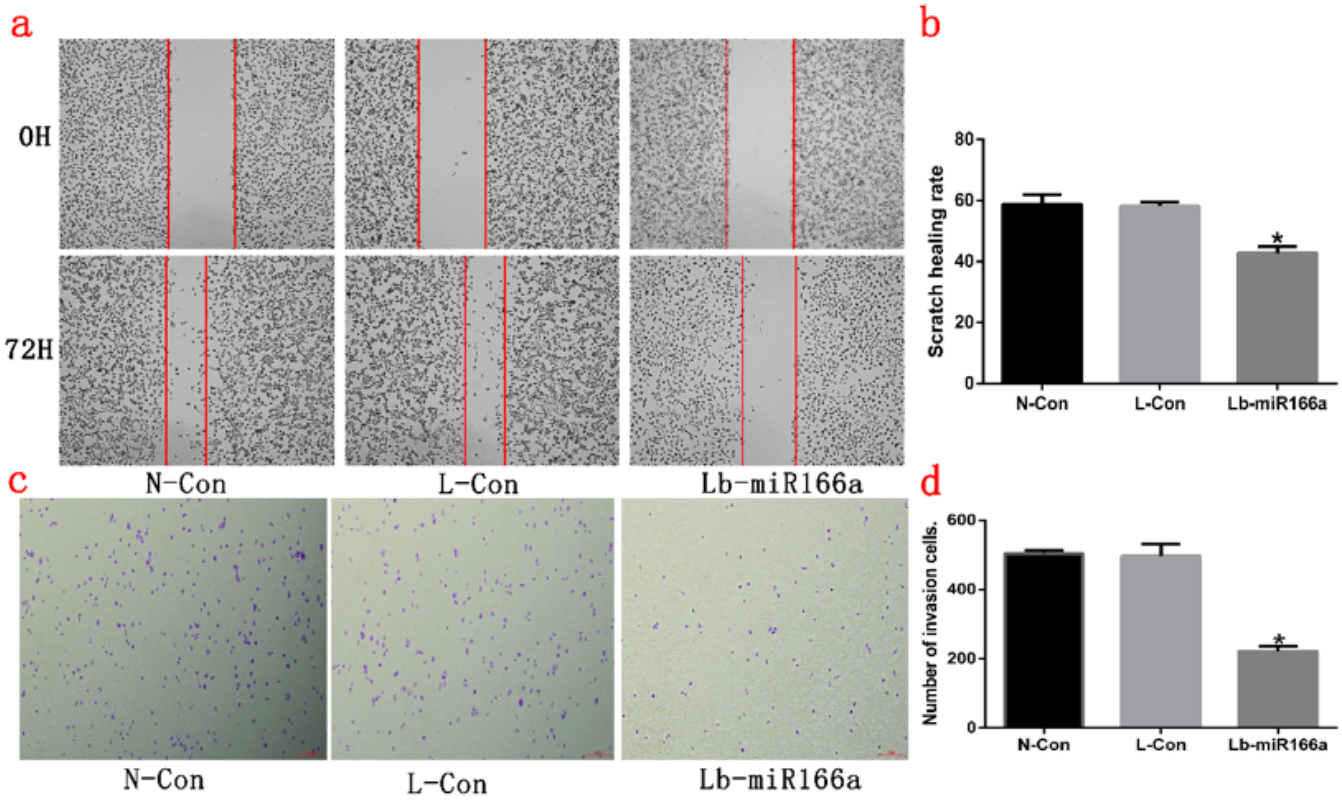

Figure 10

Lb-miR166a inhibited the migration and invasion of renal cell carcinoma cells. a,b, cell scratch test verified the effect of *Lb*-miR166a on the migration of renal cell carcinoma cells .c,b, Transwell experiment verified the effect of *Lb*-miR166a on the invasion of renal cell carcinoma cells. (*P0.05).

Figure 11

Tumor bearing experiment in nude mice . a,b,subcutaneous tumorigenesis in nude mice, tumor volume comparison . c,d, detection of the number of tumor liver metastases by tail vein injection in nude mice . e,f, Immunohistochemical expression of Ki67 in subcutaneous tumorigenesis of nude mice . (*P0.05).

Supplementary Files

This is a list of supplementary files associated with this preprint. Click to download.

- SupplementaryTable.docx